Available online at www.sciencedirect.com
ScienceDirect
International Journal of Heat and Mass Transfer 51 (2008) 3712–3723
International Journal of HEAT and MASS TRANSFER
www.elsevier.com/locate/ijhmt

Analysis of transport phenomena within PEM fuel cells – An analytical solution

Mehrzad Khakpour, Kambiz Vafai *

Mechanical Engineering Department, University of California, Riverside, CA 92521, USA

Received 24 October 2007; received in revised form 19 December 2007
Available online 4 March 2008

Abstract

Transport phenomena within PEM fuel cells are investigated and a comprehensive analytical solution is presented. The methodology couples the transport within the fuel cell supply channels and the substrate which is composed of five different layers. The layers are all treated as macroscopically homogeneous porous media with uniform morphological properties such as porosity and permeability. The locally volume-averaged equations are employed to solve for transport through the porous layers. The problem encompasses complex interfacial transport phenomena involving several porous–porous as well as porous–fluid interfaces. Chemical reactions within the catalyst layers are also included. The method of matched asymptotic expansions is employed to solve for the flow field and species concentration distributions. Throughout the analysis, the choice of the gauge parameters involved in the perturbation solutions for velocity and concentration is found to be inherently tied to the physics of the problem and therefore an important physical metric. The analytical solution is found to be in excellent agreement with prior computational simulations. The analytical results are used to investigate several aspects of transport phenomena and their substantial role in PEM fuel cell operation. The solution presented in this work provides the first comprehensive analytical solution representing fuel cell transport phenomena.

Keywords: Fuel cell; PEM; Transport phenomena; Porous media; Analytical solution

1. Introduction

Fuel cell technology has been receiving increasingly more attention as one of the most sought-after solutions to the energy and environmental pollution issues [1]. A fuel cell is an electrochemical energy device. It generates electricity through direct conversion of chemical energy of the fuel. Generally, a fuel cell consists of an anode, cathode, and an electrolyte between them. The electrochemical reactions in fuel cells happen simultaneously on both sides of the electrolyte. Fuel is oxidized within the anode. The resulting protons pass through the electrolyte towards the cathode while the electrons flow through an external circuit towards cathode, where they are needed for reduction of the oxidant [2].

Over the years, several designs of fuel cells have been proposed [2]. One of the most promising fuel cell designs is proton exchange membrane (PEM) fuel cells, also known as polymer electrolyte membrane fuel cells [2]. A schematic illustration of a PEM fuel cell is shown in Fig. 1. In this design, a polymer membrane is utilized as the electrolyte. The membrane is permeable to protons but it does not conduct electrons as this would, in effect, short-circuit the fuel cell. The membrane must also prevent either fluid (fuel or oxidant) to pass to the other side. The proton exchange membrane is sandwiched between two catalyst layers (CL). These layers are the regions where the chemical reactions take place. Catalysts lessen the activation energy, allowing the reaction to proceed more quickly or at a lower temperature. Each catalyst layer facilitates a half reaction (oxidation or reduction). These layers must allow transport of reactants, ions, electrons, and other species to support electrochemical reactions while providing a large catalyst

* Corresponding author. Tel.: +1 951 827 2135; fax: +1 951 827 2899.
E-mail address: vafai@engr.ucr.edu (K. Vafai).

0017-9310/$ - see front matter © 2008 Elsevier Ltd. All rights reserved.
doi:10.1016/j.ijheatmasstransfer.2007.12.013

Nomenclature

C	species concentration
D	mass diffusion coefficient
Da	Darcy number
F	dimensionless inertia coefficient
$\vec{J}$	unit vector oriented along the velocity vector
K	permeability
c	non-dimensional concentration
n	direction normal to interface
p	pressure
h	Width of the supply channel Reynolds number $Re_{ch} = \left(u_{ch}\sqrt{K}\right)/\nu_f$
Sc	Schmidt number
$U_{0,i}$	streamwise velocity at the ith interface
u_i	streamwise component of velocity field in ith media
u_c	Darcian convective velocity
$\vec{V}$	velocity vector
v	filtration velocity
x	axial location
y	radial location

Greek symbols

ε	Gauge parameter
ρ	density
δ	porosity
μ	dynamic viscosity
ξ	non-dimensional axial location
η	non-dimensional radial location

Subscripts

e	effective property
f	fluid
s	species field
t	total
m	momentum field
i	index $i = 0,1,\ldots,6$ representing fuel supply channel, anode GDL, anode catalyst layer, PEM, cathode catalyst layer, cathode GDL, oxidant supply channel

Symbol

$\langle\rangle$	"local volume average" of a quantity

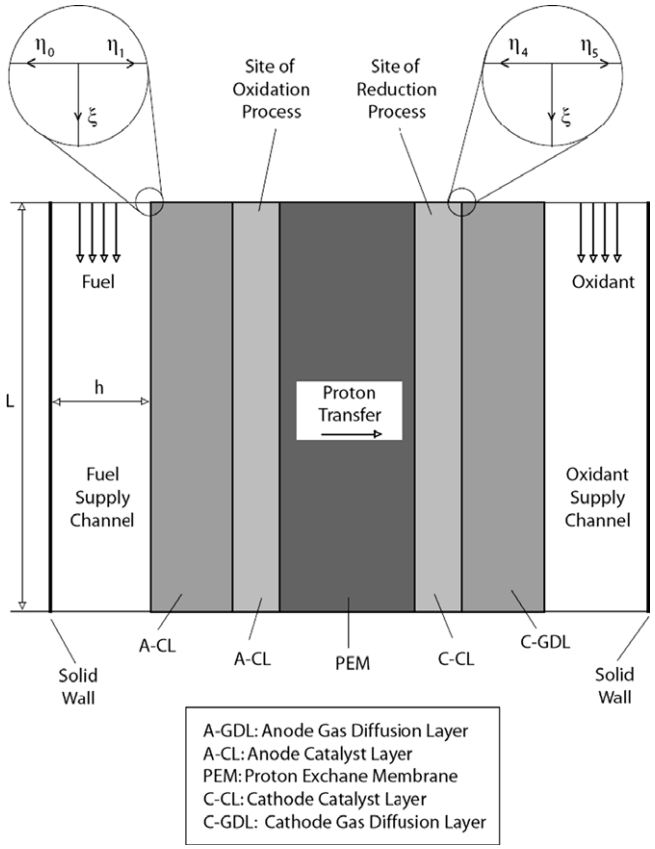

Fig. 1. Schematic illustration of a PEM fuel cell.

surface area to promote these reactions. To meet these requirements porous materials are employed.

In contact with the catalyst layers are the gas diffusion layers (GDL). PEM fuel cells require an excellent electronic contact between anode and cathode catalyst layers and gas diffusion layers. Gas diffusion layers are crucial in achieving high performance in PEM fuel cells. An ideal GDL must possess a number of characteristics such as effective transportation of gaseous reactants to the catalyst layers, proper level of hydrophobicity, and low electronic resistivity. They also play a crucial role in removing water (a byproduct of the chemical reaction) from the anode. Unlike batteries, which are closed energy storage systems, fuel cells consume reactants; thus requiring constant flow of reactants and byproducts in and out of the system, respectively. Two channels provide the reactants to different sides of this multi-layer porous substrate. Unused reactants and the reaction byproducts leave the system via the exit ports at the end of the channels.

Transport within fuel cells encompasses complex interfacial interactions between the supply channels and the porous layers [3]. In addition, it involves multi-species transport as well as oxidation/reduction chemical reactions. The impact of the velocity field on reactant transport has not received proper attention in the literature. As shown in Fig. 1, the reactants within the supply channels flow parallel to the porous structure. This induces streamwise convective transport within the porous layers. In addi-

tion, a slight pressure difference between the fuel and oxidant channels triggers a filtration phenomenon (pressure-driven convection of fuel towards the anode). The diffusion process also acts in the direction normal to the porous plates. As such, the PEM fuel cell transport phenomenon is best described by a two dimensional convective–diffusive process. This is a fact omitted in a great majority, if not all, of the existing analytical solutions [4].

Several analytical and numerical studies have been performed investigating various aspects of transport within PEM fuel cells [5–25]. While a great majority of these studies have used numerical tools, a few analytical investigations have also been attempted. Although the existing analytical solutions [4] provide some useful insight into the fuel cell transport phenomenon, they are rather simplified, omitting some key physical aspects. As mentioned earlier, their major drawback is to reduce the problem to a one dimensional diffusion problem, neglecting the tangential and transverse convective transport. Another shortcoming of the existing analytical solutions is the substantial over-simplification of fuel cell attributes, such as not properly accounting for the multi-layer specification of the PEM fuel cell structure. As such, there remains a need for a comprehensive analytical solution representing the fuel cell transport phenomena while incorporating diffusive as well as convective transport in both normal and axial directions.

In the present work, a robust theoretical solution for the species (reactant) transport within a PEM fuel cell is presented. First, the governing equations are presented. Next, a comprehensive fluid flow and mass transfer analysis is performed at each interface. The method of matched asymptotic expansion along with Laplace transformation is employed to solve for the coupled transport phenomena within supply channels and the porous structures. Using the transport parameters available in the literature, the analytical results are then compared with those obtained via numerical simulations. The solution is then used to study some of the important transport aspects of the PEM fuel cells. Our presented analytical solution is general in nature and includes two-dimensional convective and diffusive transport within the fuel cell's multi-layer structure. It can easily be extended to different models composed of any number of layers making up the fuel cell porous structure.

2. Formulation

Fig. 1 shows a schematic of a PEM fuel cell comprising seven subregions: fuel channel, anode gas diffusion layer (A-GDL), anode catalyst layer (A-CL), proton exchange membrane (PEM), cathode catalyst layer (C-CL), cathode gas diffusion layer (C-GDL), and the oxidant channel. The supply channel entrance and exit effects are considered to be negligible in the overall operation of a fuel cell. As such, the flow of reactants within the supply channels is assumed to be fully developed. Steady state, Newtonian, isothermal and incompressible flow of reactants within a fuel cell is assumed. Fluid properties (e.g. diffusivity) are assumed to remain constant. Navier–Stokes equations coupled with mass transport equations (advection–diffusion) are employed to solve for the flow of reactants within the supply channels. The governing equations for the supply channels are given by

$$\nabla \cdot \vec{V} = 0, \tag{1}$$

$$\rho \vec{V} \cdot \nabla \vec{V} = -\nabla p + \mu \nabla^2 \vec{V}, \tag{2}$$

$$\vec{V} \cdot \nabla c = D \nabla^2 c, \tag{3}$$

where $\vec{V}$ is the velocity vector, p the pressure, ρ the density, μ dynamic viscosity of the reactant, c the molar concentration, and D is the mass diffusivity of species. Due to complex nature of the interfacial transport phenomena, the inertial and boundary effects need to be accounted for [26–28]. As such, the volume-averaged equations of transport through porous media are used to solve for the flow and species fields. The governing equations for the porous layers are given by [26–28]

$$\nabla \cdot \langle \vec{V} \rangle = 0, \tag{4}$$

$$\frac{\mu}{\delta} \nabla^2 \langle \vec{V} \rangle - \frac{\mu}{K} \langle \vec{V} \rangle - \frac{\rho_f F \delta}{\sqrt{K}} \left[\langle \vec{V} \rangle \cdot \langle \vec{V} \rangle \right] \vec{J} - \nabla \langle P \rangle^f = 0, \tag{5}$$

$$\langle \vec{V} \rangle \cdot \nabla \langle c \rangle = D_e \nabla \langle c \rangle^2 + \langle S \rangle. \tag{6}$$

Here ρ_f is the fluid density, δ porosity of the porous medium, F dimensionless inertia coefficient, K is the permeability of the porous medium, and D_e represents the effective reactant diffusivity in the porous medium, respectively. The chemical reaction (source or sink) term, S, is effective only within the catalyst layers and takes a value of zero within channels, gas diffusion layers, and the proton exchange membrane. The symbol $\langle\,\rangle$, represents the local volume average of a quantity associated with the fluid. The parameters $\langle P \rangle^f$ and $\vec{J}$ are the average pressure inside the fluid and a unit vector oriented along the velocity vector $\vec{V}$, respectively [26–28].

A continuity boundary condition is employed at the interface between the layers. This boundary condition requires the value of velocity and its derivative (equivalent to shear stress) to remain constant across the interface. Similarly, the value of species concentration and the total species flux must remain constant across the interface. At the inlet a uniform and constant species concentration is prescribed.

In what follows, the method of matched asymptotic expansions is used to solve for the flow field and species concentration distributions. First, two adjacent media and the interface between them are considered. The coordinate systems are positioned at the interface between the two media. It should be noted that due to the nature of the methodology, several coordinate systems are introduced and used throughout the analysis. The normal coordinates are non-dimensionalized using appropriate gauge parameters. This is done to focus on the variations within

the close proximities of the interface. The dependent variables of interest (velocity or species concentration) are expanded in terms of powers of gauge parameters. Throughout the analysis, the choice of the gauge parameters involved in the perturbation solutions for velocity and concentration is found to be inherently tied to the physics of the problem and therefore an important physical metric. This leads to the use of a number of different gauge functions in the analysis of the fluid mechanics and different concentration distributions within different porous substrates of a PEM fuel cell.

3. Fluid flow analysis

3.1. Fluid flow within supply channel and GDL

In this part, the supply channel, its corresponding GDL, and the interface between them are considered. The coordinate system is chosen to lie at the channel-GDL interface, as shown in Fig. 1. Since there is no active transport in third direction, the problem has been reduced to two dimensions. Solving the Navier–Stokes equations using the interface fluid velocity at the fluid-porous medium interface and a no-slip boundary condition on the solid wall, the velocity profile within the channel is found to be

$$u_0 = -\eta_{\mathrm{m},0}^2 + (1 - U_{0,1})\eta_{\mathrm{m},0} + U_{0,1}, \tag{7}$$

where $\eta_{\mathrm{m},0} = y_0/h$ is the non-dimensional normal coordinate for the channel of width h, as shown in Fig. 1. It should be noted that we are also accounting for the normal component of the channel velocity when solving for the species distribution within close proximities of the channel-GDL interface. u_0 and $U_{0,1}$ are the non-dimensionalized streamwise velocities within the channel and at the channel-GDL interface, respectively. It should be noted that at this stage the interface velocity, $U_{0,1}$, is unknown. It will be found through evaluation of the velocity field within the GDL, which is governed by Eqs. (4) and (5). By introducing the gauge parameter $\varepsilon_{\mathrm{m},1} = \frac{1}{h}\sqrt{K_1/\delta_1}$ in the generalized equation of transport through GDL, it becomes

$$\frac{\mathrm{d}^2 u_1}{\mathrm{d}\eta_{\mathrm{m},1}^2} - u_1 - \alpha_1 u_1^2 + 2\delta_1 \varepsilon_{\mathrm{m},1}^2 = 0, \tag{8}$$

where u_1 is the nondimensional streamwise component of velocity within GDL and $\eta_{\mathrm{m},1}$ is the non-dimensional normal coordinate for GDL given by $\eta_{\mathrm{m},1} = y_1/\sqrt{K_1/\delta_1}$. The parameter α_1 is given as $\alpha_1 = F_1\delta_1 Re_{\mathrm{ch},1}$ where the Reynolds number is calculated based on characteristic velocity and the permeability of the porous medium, $Re_{\mathrm{ch},1} = \left(u_{\mathrm{ch},0}\sqrt{K_1}\right)/\nu_{\mathrm{f}}$. The non-dimensional streamwise component of velocity vector within the GDL, $u_1 = \langle u_1\rangle / u_{\mathrm{ch},0}$, is expanded in terms of the powers of the gauge parameter as

$$u_1 = \varepsilon_{\mathrm{m},1}u_{1,1} + \varepsilon_{\mathrm{m},1}^2 u_{1,2} + \varepsilon_{\mathrm{m},1}^3 u_{1,3} + \cdots \tag{9}$$

Using the method of matched asymptotic expansions, the first three orders of the inner solution for GDL are found to be

$$u_{1,1} = \exp(-\eta_{\mathrm{m},1}^*), \tag{10}$$

$$u_{1,2} = \frac{\alpha_1}{3}\exp(-2\eta_{\mathrm{m},1}^*) - \left(\frac{2\alpha_1}{3} + 1\right)\exp(-\eta_{\mathrm{m},1}^*) + 2\delta_1, \tag{11}$$

$$u_{1,3} = \frac{\alpha_1^2}{12}\exp(-3\eta_{\mathrm{m},1}) - \frac{2\alpha_1}{3}\left(\frac{2\alpha_1}{3} + 1\right)\exp(-2\eta_{\mathrm{m},1}) + \left[\left(1 - 2\delta_1 + \frac{5\alpha_1}{3} + \frac{23\alpha_1^2}{36} - \alpha_1\delta_1\right) - 2\alpha_1\delta_1\eta_{\mathrm{m},1}\right]\exp(-\eta_{\mathrm{m},1}). \tag{12}$$

By setting $\eta_{\mathrm{m},1} = 0$, the interface velocity is found to be

$$U_{0,1} = \varepsilon_{\mathrm{m},1} + \left(2\delta_1 - 1 - \frac{\alpha_1}{3}\right)\varepsilon_{\mathrm{m},1}^2 + \left(\frac{5\alpha_1^2}{18} + (1 - \delta_1)\alpha_1 - 2\delta_1 + 1\right)\varepsilon_{\mathrm{m},1}^3. \tag{13}$$

Inserting Eq. (13) into Eq. (7) gives the velocity profile within the supply channel.

3.2. Fluid flow within the porous layers

A schematic of the coordinate system used in the calculation of the velocity profile within two neighboring porous media (e.g. GDL and catalyst layer) is presented in Fig. 1. First, the governing equations are non-dimensionalized using the Darcian convective velocity given as

$$u_{\mathrm{c},i} = -\frac{K_i}{\mu_{\mathrm{f}}}\left(\frac{\mathrm{d}\langle p_i\rangle^{\mathrm{f}}}{\mathrm{d}x}\right), \tag{14}$$

where the subscript i refers to the ith porous medium. The generalized equation of transport through the two porous media reduces to

$$\frac{\mathrm{d}^2 u_i}{\mathrm{d}\eta_{\mathrm{m},i}^2} - u_i - \alpha_i u_i^2 + 1 = 0. \tag{15}$$

The velocities, u_i, are expanded in terms of powers of porosities, δ_i, as

$$u_i = u_{i,0} + \delta_i u_{i,1} + \delta_i^2 u_{i,2} + \cdots \tag{16}$$

The outer solution, u_i^*, for the catalyst layer is found to be

$$u_2^* = 1 - \beta_2\delta_2 + 2\beta_2^2\delta_2^2 - 5\beta_2^3\delta_2^3 + \cdots \tag{17}$$

The solutions for the first three orders of the inner solution for catalyst layer are calculated to be

$$u_{2,0} = 1 + (U_{2,0} - 1)\exp(-\eta_{\mathrm{m},2}), \tag{18}$$

$$u_{2,1} = U_{2,1}\exp(-\eta_{\mathrm{m},2}) + \beta_2\left(-1 + \exp(-\eta_{\mathrm{m},2})[1 - \eta_{\mathrm{m},2}(U_{2,0} - 1) - 1/3(U_{2,0} - 1)^2] + 1/3\exp(-2\eta_{\mathrm{m},2})(U_{2,0} - 1)^2\right), \tag{19}$$

$$u_{2,2} = U_{2,2}\exp(-\eta_{m,2}) + \beta_2 U_{2,1}\big(-\exp(-\eta_{m,2})[\eta_{m,2} + 2/3(U_{2,0}-1)] + 2/3\exp(-2\eta_{m,2})(U_{2,0}-1)\big) + \beta_2^2\big(2+\exp(-\eta_{m,2})[A_2\eta_{m,2}^2 + B_2\eta_{m,2} + C_2] + \exp(-2\eta_{m,2})[4/3A_2\eta_{m,2} + D_2] + 1/12\exp(-3\eta_{m,2})(U_{2,0}-1)^3\big), \quad (20)$$

where $\beta_2 = F_2 Re_2$ and

$$A_2 = 1/2(U_{2,0}-1)^2, \quad (21)$$

$$B_2 = 1/3(U_{2,0}-1)^2 + 3/2(U_{2,0}-1) - 1, \quad (22)$$

$$C_2 = 5/36(U_{2,0}-1)^3 + 2/3(U_{2,0}-1)^2 - 2/3(U_{2,0}-1) - 2, \quad (23)$$

$$D_2 = 2/3(U_{2,0}-1)[1-(U_{2,0}-1) - 1/3(U_{2,0}-1)^2]. \quad (24)$$

An explicit expression for the interface velocity will now be obtained using the continuity of velocity and the shear stress across the interface

$$U_{2,0} = \frac{1+(r_1/r_2)^{1/2}(r_1r_3)^{-1}}{1+(r_1/r_2)^{1/2}}, \quad (25)$$

$$U_{2,1} = -\frac{\beta_2(\phi_1+\phi_2+\phi_3)}{3(1+(r_1/r_2)^{1/2})}, \quad (26)$$

$$U_{2,2} = \frac{(\beta_2)^2(\phi_4+\phi_5)+\beta_2(-2\phi_1-\phi_2)}{3(1+(r_1/r_2)^{1/2})}, \quad (27)$$

$$\phi_1 = (1+(r_4r_2^{3/2})^{-1})(U_{2,0})^2, \quad (28)$$

$$\phi_2 = (1+(r_1r_4r_3r_2^{3/2})^{-1})U_{2,0}, \quad (29)$$

$$\phi_3 = 1+(r_1^2r_3^2r_4r_2^{3/2})^{-1}, \quad (30)$$

$$\phi_4 = (1+(r_1^{1/2}r_2^{5/2}r_4^2)^{-1})(U_{2,0})^3 + (1+(r_1^{3/2}r_2^{5/2}r_3r_4^2)^{-1})(U_{2,0})^2, \quad (31)$$

$$\phi_5 = (1+(r_1^{5/2}r_2^{5/2}r_3^2r_4^2)^{-1})U_{2,0} + (1+(r_1^{7/2}r_2^{5/2}r_3^3r_4^2)^{-1}), \quad (32)$$

where $r_1 = \frac{K_1}{K_2}, r_2 = \frac{\delta_1}{\delta_2}, r_3 = \frac{(dp/dx)_1}{(dp/dx)_2}, r_4 = \frac{F_1}{F_2}$ are the ratios of the basic properties of the two porous media. A similar approach is used to obtain the velocity distribution within the proton exchange membrane. It has been shown that the inertial and boundary effects have negligible effects on the calculation of filtration velocity across a multi-layer porous plate. As such, Darcy's law is employed to calculate the filtration velocity (velocity of the fluid moving from anode towards cathode) across the porous substrate. Applying Darcy's law to the multi-layer porous structure and observing the continuity of the filtration velocity across the layers, we get

$$v = -\frac{K_t}{\mu_f}\frac{dp}{dn}, \quad (33)$$

where v is the filtration velocity, $\frac{dp}{dn}$ is the pressure gradient across the multi-layer porous substrate with a permeability of K_t given by

$$K_t = \frac{l_t}{\sum_i \frac{l_i}{K_i}} \quad (34)$$

where the index i represents the porous layers and l_t is the total thickness of the arterial wall.

4. Mass transfer analysis

The PEM fuel cell operation is based on the premise that the fuel (e.g. hydrogen) is found within the fuel supply channel, the anode gas diffusion layer, and the anode catalyst layer. Along the anode catalyst layer hydrogen undergoes an oxidation process to produce protons which can permeate into the proton exchange membrane towards cathode catalyst layer. The proton exchange membrane does not permeate hydrogen. It is assumed that all the protons are consumed within the cathode catalyst layer, thus no protons penetrate into the cathode GDL. The oxidant diffuses into the cathode gas diffusion layer, reaching the cathode catalyst layer, where it is completely consumed through interaction with the penetrating protons. In addition, the proton exchange membrane is impermeable to the oxidant as well. These attributes are the operational characteristics of a PEM fuel cell, which are utilized to prescribe an appropriate set of species boundary conditions for the subsequent analytical solution. In this section, comprehensive analytical solutions are obtained for concentration distributions within various porous substrates comprising the PEM fuel cell. The governing species conservation equation was presented earlier in its general form as Eqs. (3) and (6) for a channel and a porous substrate, respectively. The method of matched asymptotic expansions is used to solve for the concentration fields.

4.1. Mass transport within supply channel and GDL

In this part, the supply channel, its corresponding GDL, and the interface between them are considered. The coordinate system is located at the interface, as shown in Fig. 1. In the vicinity of the interface, it is assumed that the transverse component of the velocity vector within the channel remains constant and equal to the filtration velocity. Inside the concentration boundary layer, we are interested in small values of η_m. This suggests expansions of the streamwise component of the velocity vector for small values of η_m as shown here

$$u_0 = U_{0,1} + (1-U_{0,1})\eta_{s,0}Sc_0^{-1/2}\sqrt{K/h^2}, \quad (35)$$

$$U_{0,1} = \varepsilon_{m,1} + \left(2\delta_1 - \frac{\alpha_1}{3} - 1\right)\varepsilon_{m,1}^2 + \left(1 - 2\delta_1 + \alpha_1\delta_1 + \alpha_1 + \frac{5\alpha_1^2}{18}\right)\varepsilon_{m,1}^3, \quad (36)$$

$$u_1 = (1-\eta_{s,1}Sc_1^{-1/2})\varepsilon_{m,1} + \left[\left(2\delta_1 - \frac{\alpha_1}{3} - 1\right) - \eta_{s,1}Sc_1^{-1/2}\right]\varepsilon_{m,1}^2 + \left[\left(1 - 2\delta_1 + \alpha_1\delta_1 + \alpha_1 + \frac{5\alpha_1^2}{18}\right) - \left(1 - 2\delta_1 + \alpha_1\delta_1 + \alpha_1 + \frac{4\alpha_1^2}{9}\right)\eta_{s,1}Sc_1^{-1/2}\right]\varepsilon_{m,1}^3, \quad (37)$$

where Sc_i is the reference Schmidt number in the ith medium defined as the larger of the Schmidt numbers of the two species, $Sc_i = \mathrm{Max}\{Sc_i^1, Sc_i^2\}$. Recall that the subscripts 0 and 1 refer to the supply channel and GDL, respectively. The parameter $U_{0,1}$ represents the streamwise velocity profile along the channel-GDL interface. This is done to employ the same coordinate system for both species and is helpful in the solution of mass concentrations which are coupled via the source/sink terms. Also note that a new set of coordinate system and spatial variables are introduced. Here, $\eta_{s,0}$ and $\eta_{s,1}$ represent the non-dimensional coordinates used in the mass transfer analysis and are given by

$$\eta_{s,i} = y_i/\varepsilon_{s,i} = y_i\sqrt{\frac{\delta_i Sc_i}{K_1}}, \tag{38}$$

where again $i = 0$ and 1 represents supply channel and GDL, respectively. Note that the porosity of supply channel is unity. Using the coordinate transformation and the velocity distribution given in Eqs. (35)–(37), the species conservation equation for channel and GDL are written as

$$-V\frac{\partial c_0^j}{\partial \eta_{\mathrm{s},0}} + \left[U_0 + (1-U_0)\eta_{\mathrm{s},0}Sc_0^{-1/2}\sqrt{K/h^2}\right]\frac{\partial c_0^j}{\partial \xi} = \frac{1}{Re_{\mathrm{ch},0}\sqrt{Da_1}}\frac{\partial^2 c_0^j}{\partial \eta_{\mathrm{s},0}^2}, \tag{39}$$

$$V\frac{\partial c_1^j}{\partial \eta_{\mathrm{s},1}} + [U_{0,1} + \eta_{\mathrm{s},1}Sc_1^{-1/2}\Lambda_1]\frac{\partial c_1^j}{\partial \xi} = \frac{1}{Re_{\mathrm{ch},1}\sqrt{Da_1}}\frac{\partial^2 c_1^j}{\partial \eta_{\mathrm{s},1}^2}, \tag{40}$$

$$\Lambda_1 = -\left[\varepsilon_{\mathrm{m},1} + \varepsilon_{\mathrm{m},1}^2 + \left(1 - 2\delta_1 + \alpha_1\delta_1 + \alpha_1 + \frac{4\alpha_1^2}{9}\right)\varepsilon_{\mathrm{m},1}^3\right], \tag{41}$$

where $\xi = x/L$. Note that in the channel within close proximities of the channel-GDL interface, the normal component of velocity is assumed to be constant and equal to that of filtration within the GDL [29]. The corresponding boundary condition are given as

$$c_i^j(\xi = 0, \eta_{s,i}) = 0, \tag{42}$$

$$c_i^j(\xi, \eta_{s,i} = 0) = f_i^j(\xi), \tag{43}$$

where c_i^j is the non-dimensional concentration of species j within ith media given by

$$c_i^j = \frac{C_i^j - C_{\infty,i}^j}{C_{\mathrm{ref}}^j}, \tag{44}$$

where $C_{\infty,i}^j$ is the concentration of species j within medium i at an axial location of $\xi = 0$. Also C_{ref}^j is the reference concentration of species j used for nondimensionalization. The concentration field is expanded in terms of $Sc_i^{-1/2}$ as

$$c_i^j(\xi, \eta_{\mathrm{s},i}) = c_{i,0}^j(\xi, \eta_{\mathrm{s},i}) + c_{i,1}^j(\xi, \eta_{\mathrm{s},i})Sc_i^{-1/2} + \cdots \tag{45}$$

with the nondimensional interface concentration expanded as

$$f_i^j(\xi, \eta_{\mathrm{s},i}) = f_{i,0}^j(\xi) + f_{i,1}^j(\xi)Sc_i^{-1/2} + \cdots \tag{46}$$

As mentioned before, the interface concentration itself is obtained using the continuity conditions for both mass concentration and flux. Using the method of matched asymptotic expansion and Laplace transforms, the first- and second-order concentration distributions in the GDL are found to be

$$c_{1,0}^j(\xi, \eta_{\mathrm{s},1}) = f_{1,0}^j\exp(A_1)\left[\left(1 + \frac{B_1^2E_1}{2}\right)\mathrm{erfc}\left(\frac{B_1}{2\sqrt{\xi}}\right) - \frac{B_1E_1}{\sqrt{\pi}}\sqrt{\xi}\exp\left(-\frac{B_1^2}{4\xi}\right)\right], \tag{47}$$

$$c_{1,1}^j(\xi, \eta_{\mathrm{s},1}) = \frac{f_{1,1}^j\exp(A_1)}{8}\left[(8 + 2B_1^2E_1)\sqrt{\xi}\exp\left(-\frac{B_1^2}{4\xi}\right) - B_1E_1\sqrt{\pi}(4 + B_1^2 + 2\xi)\mathrm{erfc}\left(\frac{B_1}{2\sqrt{\xi}}\right)\right] + \frac{f_{1,0}^j\Lambda_1\exp(A_1 - E_1\xi)\eta_{\mathrm{s},1}^3}{4\sqrt{\pi}B_1^2\sqrt{\xi}} \times \left[B_1\exp\left(-\frac{B_1^2}{4\xi}\right) - \mathrm{erfc}\left(\frac{B_1}{2\sqrt{\xi}}\right)\right], \tag{48}$$

where

$$A_1 = \frac{V\eta_{\mathrm{s},1}}{2Q_1}, \tag{49}$$

$$B_1 = \eta_{\mathrm{s},1}\sqrt{U_{0,1}/Q_1}, \tag{50}$$

$$E_1 = \frac{V^2}{4U_{0,1}Q_1}, \tag{51}$$

$$Q_1 = \frac{1}{Re_{\mathrm{ch},1}\sqrt{Da_1}}. \tag{52}$$

4.2. Species transport within GDL and catalyst layer while accounting for a chemical reaction

As mentioned earlier, the porous substrate used in PEM fuel cells is generally composed of five layers, two of which undergo chemical reactions. As seen in Fig. 1, taking every two neighboring porous layers, one of them includes a chemical reaction. The reaction within the anode catalyst layer is an oxidation process. It has been shown that in hydrogen PEM fuel cells, usually very low polarization occurs at the anode due to the fast hydrogen oxidation. In other words, the cell performance is not likely to be limited by the hydrogen oxidation kinetics, because it is very fast (at least five orders of magnitude) compared to that of oxygen reduction at the cathode. Therefore, most of the attention in the literature has been focused on oxygen gas transport through the cathode region of PEM fuel cells.

The hydrogen oxidation process can be modeled as a simple first-order chemical reaction with a constant reaction rate. Within the cathode catalyst layer however, the chemical reaction is a reduction process which involves two species. As such, the reaction process is inherently second-order thus dependent upon the concentration of both species. Exact solution of the species conservation equation with a second-order chemical reaction is extremely cumbersome, if not impossible. Therefore, the reduction half reaction is also modeled as a simple first-order chemical reaction. A discussion of the effects of this assumption is presented later on.

In this part, two adjacent porous media and the interface between them are considered. It is assumed that one of the media undergoes an irreversible first-order chemical reaction with a constant reaction rate. The corresponding concentration fields, c_1^j and c_2^j, are expanded according to Eq. (45). Using a coordinate system similar to that presented in Fig. 1, the species conservation equation within the reaction-less medium (e.g. GDL) is given by

$$-V\frac{\partial c_1^j}{\partial \eta_{s,1}}+\left[U_{0,2}+\Lambda_1\eta_{s,1}Sc_1^{-1/2}\right]\frac{\partial c_1^j}{\partial \xi}=\frac{1}{Re_{ch,1}\sqrt{Da_1}}\frac{\partial^2 c_1^j}{\partial \eta_{s,1}^2}. \tag{53}$$

The species conservation equation within the reacting medium (e.g. catalyst layer) is given by

$$V\frac{\partial c_2^j}{\partial \eta_{s,2}}+\left[U_{0,2}+\Lambda_2\eta_{s,2}Sc_2^{-1/2}\right]\frac{\partial c_2^j}{\partial \xi}=\frac{1}{Re_{ch,2}\sqrt{Da_2}}\frac{\partial^2 c_2^j}{\partial \eta_{s,2}^2}-r_2^j c_2^j-R_2^j, \tag{54}$$

where r_2^j is the non-dimensional chemical reaction rate given as

$$r_2^j=\frac{k_2^j\varepsilon_{s,2}}{u_{ch,0}}. \tag{55}$$

The term R_2^j is the residue of the non-dimensionalization process of the reaction term and is given by

$$R_2^j=\frac{k_2^j C_{\infty,2}^j\varepsilon_{s,2}}{u_{ch,0}C_{ref}^j}, \tag{56}$$

where $C_{\infty,2}^j$ is the concentration of species j at $\xi=0$. In the case of transport within porous substrates of PEM fuel cells, $C_{\infty,2}^j$ and therefore R_2^j is equal to zero. However, to maintain the generality of our analytical solution we will carry this term through the analysis. Using the method of matched asymptotic expansions, Laplace transform in ξ domain, and the continuity of species concentration and flux at the interface, the zeroth- and first-order concentration distributions within the reacting media (catalyst layer) are found to be

$$\begin{aligned}c_{2,0}^j(\xi,\eta_{s,2})=&\left(f_{2,0}^j+\frac{R_2^j}{r_2^j}\right)\exp(A_2)\left[\left(1+\frac{(B_2)^2E_2^j}{2}\right)\mathrm{erfc}\left(\frac{B_2}{2\sqrt{\xi}}\right)\right.\\&\left.-\frac{B_2E_2^j}{\sqrt{\pi}}\sqrt{\xi}\exp\left(-\frac{(B_2)^2}{4\xi}\right)\right]-\frac{R_2^j}{r_2^j}\exp(A_2-G_2^j\xi)\\&\times\left[\left(1+\frac{(B_2)^2(E_2^j-G_2^j)}{2}\right)\mathrm{erfc}\left(\frac{B_2}{2\sqrt{\xi}}\right)\right.\\&\left.-\frac{B_2(E_2^j-G_2^j)}{\sqrt{\pi}}\sqrt{\xi}\exp\left(-\frac{(B_2)^2}{4\xi}\right)\right]\\&-\frac{R_2^j}{r_2^j}[1-\exp(-G_2^j\xi)],\end{aligned} \tag{57}$$

$$\begin{aligned}c_{2,1}^j(\xi,\eta_{s,2})=&\frac{f_{2,1}^j\exp(A_2)}{8}\left[\begin{array}{l}(8+2(B_2)^2E_2^j)\sqrt{\xi}\exp\left(-\frac{(B_2)^2}{4\xi}\right)-\\B_2E_2^j\sqrt{\pi}(4+(B_2)^2+2\xi)\mathrm{erfc}\left(\frac{B_2}{2\sqrt{\xi}}\right)\end{array}\right]\\&+\frac{\left(f_{2,0}^j+\frac{R_2^j}{r_2^j}\right)\Lambda_2\exp(A_2-E_2^j\xi)\eta_{s,2}^3}{4\sqrt{\pi}(B_2)^2\sqrt{\xi}}\left[B_2\exp\left(-\frac{(B_2)^2}{4\xi}\right)\right.\\&\left.-\mathrm{erfc}\left(\frac{B_2}{2\sqrt{\xi}}\right)\right],\end{aligned} \tag{58}$$

$$A_2=\frac{V\eta_{s,2}}{2Q_2}, \tag{59}$$

$$B_2=\eta_{s,2}\sqrt{U_{0,2}/Q_2}, \tag{60}$$

$$E_2^j=\frac{V^2+4r_2^jQ_2}{4U_{0,2}Q_2}, \tag{61}$$

$$G_2^j=\frac{r_2^j}{U_{0,2}}. \tag{62}$$

It bears mentioning that this solution is comprehensive and can be adjusted for simpler cases. For instance, setting r_2^j and R_2^j equal to zero results in the species concentration distribution within two neighboring porous media without any reactions.

5. Results and discussion

The analytical solution presented in the preceding section is compared to the available numerical results for a hydrogen–oxygen single PEM fuel cell [21]. Eqs. (7)–(34) prescribe the velocity field within the channels and the porous substrates comprising a PEM fuel cell. Note that the filtration velocity is dependent upon the existence of a pressure differential across the porous substrates. In other words, if the fuel and the oxidant are supplied with the same pressure, there will be no filtration velocity and the mass transfer process will be influenced by normal diffusion and axial convective transport only. The proper methodology for calculating the filtration velocity across a multilayer porous membrane has already been shown in the analytical work of Yang and Vafai [30] and is adopted here.

Using Eq. (34), the average permeability is found to be $K_{total} = 6.22 \times 10^{-18}$ m^2, which is of the same order of magnitude as that of proton exchange membrane. This indicates that the filtration velocity is mostly dependent on the permeability of the proton exchange membrane. For a pressure differential of $\Delta P = 2$ atm [21], the filtration velocity of hydrogen across the porous structure is calculated to be $v = 1.81 \times 10^{-4}$ m/s. Unlike the filtration velocity, the streamwise velocity is different in each layer, with proton exchange membrane and catalyst layers having the lowest and highest values, respectively. Streamwise velocity within proton exchange membrane is roughly eight orders of magnitude smaller than that within catalyst layers. Therefore, neglecting the streamwise velocity and its convective effects may be justified for proton exchange membrane but it can result in significant error in species concentration distribution within the catalyst layers, where the reactions occur.

The analytical results are used to describe the species mole fraction distributions within the porous substrate of a PEM fuel cell. The first step is to estimate a first-order chemical reaction rate. This is done via a single point data backtracking method. First, a single point from the computational results of Um et. al. [21] is chosen. Then the value of the mole fraction at the chosen point is utilized in the analytical solution. This enables evaluation of the unknown namely, the first-order reaction rate constant, from the analytical expressions. This estimated reaction rate constant is then used for the entire catalyst layer. From an electrochemical point of view, this is a simplification; however it serves well the main purpose of this study which is the analysis of fuel cell transport phenomena and its underlying interfacial interactions.

Fig. 2 shows the axial variation of hydrogen mole fraction profile along the Channel-GDL and GDL-CL interfaces on the anode side. The analytical results are in good agreement with recent computational findings [21]. At the anode channel-GDL interface, the disparity between analytical and computational results is less than 8%. The axial decrease in the hydrogen mole fraction is caused by diffusion of hydrogen from the anode stream to the cathode reaction surface where it undergoes a chemical reaction. This axial decrease (down-the-channel effect) becomes particularly significant for the high fuel utilization conditions that are needed for the highest possible fuel efficiency. This effect is of substantial importance and will not be captured by one dimensional analytical solutions.

Fig. 3 shows a representative oxygen mole fraction profile at an axial location of $x = L/2$ across C-CL and C-GDL. The results are compared against the computational findings of Um et. al. [21]. It is observed that the oxygen mole fraction profile corresponding to our estimated reaction rate of $k = 1000$ $(1/m^3)$, which was obtained via a single data back tracking for the first comparison, is in good agreement with the computational results of Um et. al. [21]. Within the C-GDL, a maximum of 6% difference is observed. At $\xi = 0.5$ along the cathode channel-GDL interface, the calculated oxygen mole fraction is roughly 0.167 and 0.173 for the computational and analytical results, respectively. The small difference may be due to the use of an approximate reaction rate constant, which can affect the depletion rate. Overall, the general trend is consistent with the computational results [21]. Due to mass transport resistance, the oxygen mole fraction further reduces across the C-GDL. The discontinuous drop at the cathode GDL-CL interface is a result of the difference

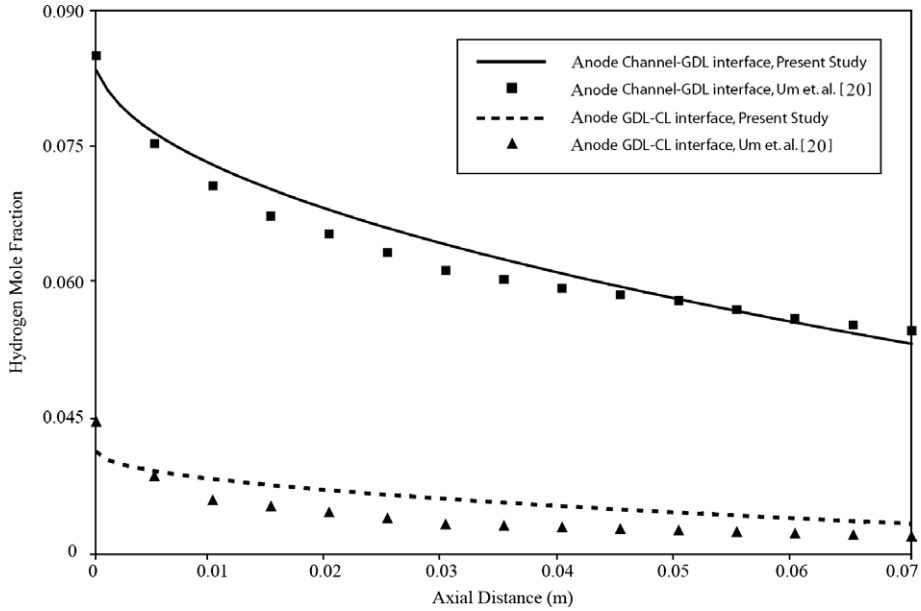

Fig. 2. Axial variation of hydrogen mole fraction profile along the channel-GDL and GDL-CL interfaces on the anode side.

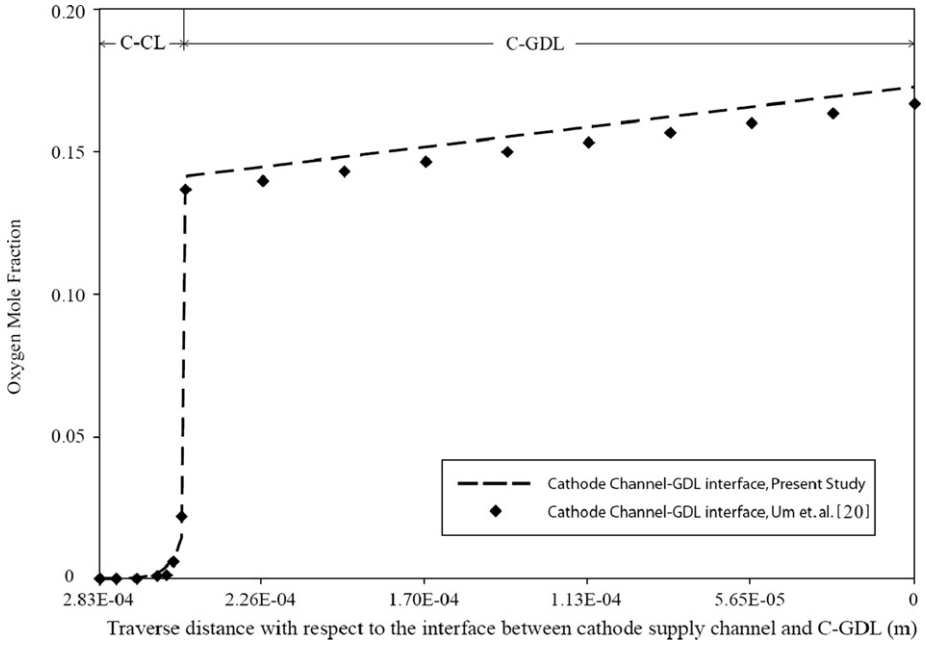

Fig. 3. Oxygen mole fraction profile across C-GDL and C-CL $\xi = 1/2$.

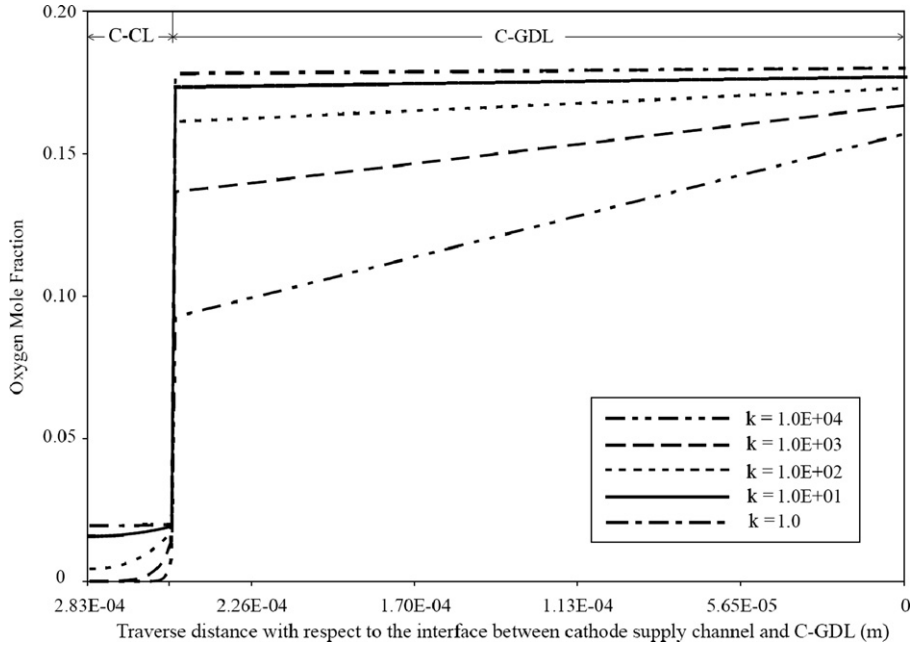

Fig. 4. Oxygen mole fraction profile across C-GDL and C-CL for different values of chemical reaction rate; $\xi = 1/2$.

between the porosities of the two media. Within the C-CL, all oxygen in the membrane phase is consumed by the oxygen reduction reaction.

Fig. 4 shows the effects of chemical reaction rate on oxygen mole fraction distributions across cathode GDL and catalyst layer. The results correspond to a filtration velocity of $v = 1.81 \times 10^{-4}$ m/s. The reaction rate affects the value of oxygen mole fraction at the cathode channel-GDL interface (down-the-channel depletion effect), and it also increases the concentration gradient within the C-GDL. This figure displays the influence of chemical reaction process on the reactants flux and their distribution within the layers. The effects of filtration velocity on oxygen mole fraction distribution are presented in Fig. 5. Two different filtration velocities are shown in combination with two different values of reaction rates.

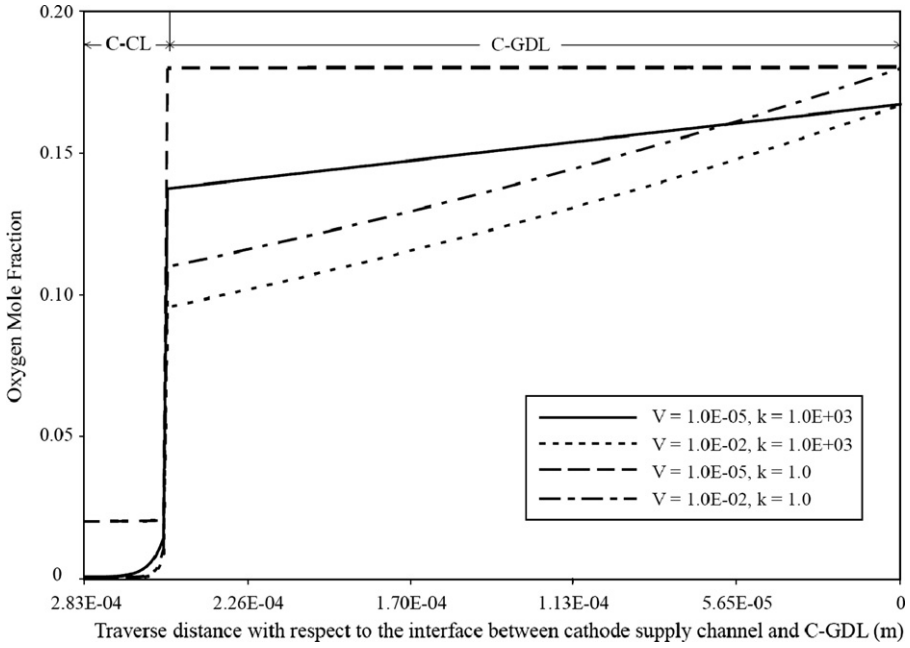

Fig. 5. Oxygen mole fraction profile across C-GDL and C-CL for different values of filtration velocity and chemical reaction rate; $\xi = 1/2$.

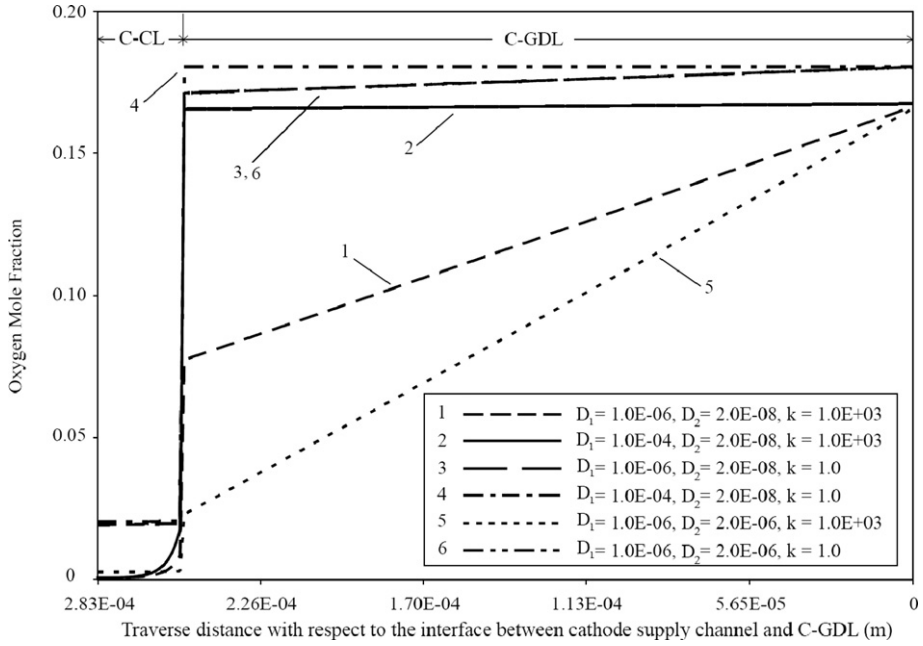

Fig. 6. Oxygen mole fraction profile across C-GDL and C-CL for different values of effective diffusion coefficient and chemical reaction rate; $\xi = 1/2$.

As expected, a larger filtration velocity towards the oxidant channel creates a steeper decrease of the oxidant across the C-GDL layer. This is due to the fact that the transport due to filtration acts against the direction of favorable oxygen delivery. This effect is more pronounced for slower reaction rates. In other words, the influence of filtration velocity on oxygen delivery becomes less important as the chemical reaction rate increases. Also, it is observed that the oxygen mole fraction at the cathode channel-GDL remains roughly the same for both values of filtration velocity.

Fig. 6 shows the importance of diffusion coefficients on oxygen delivery. The plots represent different diffusion coefficients for both C-GDL and C-CL for two different values of reaction rate. It can be seen that in case of slow chemical reaction, diffusivity within C-GDL has a small effect whereas diffusivity within C-CL has an insignificant effect on oxygen mole fraction. For the case of

higher reaction rates however, both diffusion coefficients have a substantial effect on oxygen distribution within the layers.

6. Conclusions

A theoretical analysis of transport phenomena within PEM fuel cells is performed and a comprehensive analytical solution is presented. The analysis includes both transverse and axial convective transport as well as transverse diffusive transport processes. Chemical reactions within the catalyst layers are also included. The methodology couples the transport within the fuel cell supply channels and the porous substrate. The fuel cell layers are treated as macroscopically homogeneous porous media with uniform morphological properties such as porosity and permeability. Volume-averaged porous media equations are employed to solve for transport through these porous layers. The method of matched asymptotic expansions and Laplace transformations are employed to solve for the flow field and species concentration distributions. Throughout the analysis, the choice of the gauge parameters involved in the perturbation solutions for velocity and concentration are found to be of substantial importance and inherently tied to the physics of the problem. The problem encompasses complex interfacial transport phenomena involving several porous–porous as well as porous–fluid interfaces.

The first-order chemical reaction term is estimated via a single point data backtracking method using earlier published computational results. The analytical results are in excellent agreement with previous numerical studies. The analytical solution is used to study the importance of transport phenomena in PEM fuel cell operation and their interaction with chemical reaction processes. It is shown that the rate of the chemical reaction has a substantial influence on the reactant flux and its distribution within the porous substrate. The role of filtration velocity was also discussed. Filtration velocity is triggered by a pressure differential between the fuel and oxidant supply channels. It improves fuel delivery and water removal; however it can act against the oxidant delivery depending on the direction of the pressure differential. It is shown that the transport phenomena play a substantial role on PEM fuel cell operation. The effects of filtration velocity, chemical reaction rate, and diffusivity have been discussed.

This work provides the first comprehensive analytical solution representing fuel cell transport phenomena. The presented solution can be used to analyze fuel cell operation under different conditions. It also provides a benchmark for future works on PEM fuel cells, especially those investigating transport characteristics. The present analytical solution can easily be extended to investigate different models composed of any number of layers making up the porous substrate.

References

[1] A. Stambouli, E. Traversa, Fuel cells, an alternative to standard sources of energy, Renew. Sust. Energy Rev. 6 (2002) 295–304.
[2] A. Faghri, Z. Guo, Challenges and opportunities of thermal management issues related to fuel cell technology and modeling, Int. J. Heat Mass Transfer 48 (2005) 19–20.
[3] K. Vafai, R. Thiyagaraja, Analysis of flow and heat transfer at the interface region of a porous medium, Int. J. Heat Mass Transfer 30 (1987) 1391–1405.
[4] D. Bernardi, M. Verbrugge, A mathematical model of the solid polymer electrolyte fuel cell, J. Electrochem. Soc. (1992).
[5] D. Singh, D. Lu, N. Djilali, A two-dimensional analysis of mass transport in proton exchange membrane fuel cells, Int. J. Eng. Sci 37 (1999) 431–452.
[6] V. Gurau, H. Liu, S. Kakac, A two dimensional model for proton exchange fuel cells, AIChE J. 44 (1998) 2410–2422.
[7] A. Kazim, H. Liu, P. Forges, Modelling of performance of PEM fuel cells with conventional and interdigitated flow fields, J. Appl. Electrochem. 29 (1999) 1409–1416.
[8] W. He, J. Yi, T. Nguyen, Two-phase flow model of the cathode of PEM fuel cells using interdigitated flow fields, AIChE J. 46 (2000) 2053–2064.
[9] D. Natarajan, T. Nguyen, A two-dimensional two-phase multicomponent transient model for the cathode of a proton exchange membrane fuel cell using conventional gas distributors, J. Electrochem. Soc. 148 (2001) A1324–A1335.
[10] L. You, H. Liu, A two-phase flow and transport model for the cathode of PEM fuel cells, Int. J. Heat Mass Transfer 45 (2002) 2277–2287.
[11] P. Li, L. Schaefer, Q. Wang, T. Zhang, M. Chyu, Multi-gas transportation and electrochemical performance of a polymer electrolyte fuel cell with complex flow channels, J. Power Sources 115 (2003) 90–100.
[12] H. Liu, T. Zhou, Fuel cell performance augmentation: mass transfer enhancement, J. Enhanced Heat Transfer 10 (2003) 257–274.
[13] T. Mennola, M. Noponen, M. Aronniemi, T. Hottinen, M. Mikkola, O. Himanen, P. Lund, Mass transport in the cathode of a free-breathing polymer electrolyte membrane fuel cell, J. Appl. Electrochem. 33 (2003) 979–987.
[14] T. Berning, N. Djilali, A 3D multiphase multicomponent model of the cathode and anode of a PEM fuel cell, J. Electrochem. Soc. 150 (2003) A1589–A1598.
[15] J. Nam, M. Kaviany, Effective diffusivity and water-saturation distribution in single- and two-layer PEMFC diffusion medium, Int. J. Heat Mass Transfer 46 (2003) 4595–4611.
[16] S. Mazumder, J. Cole, Rigorous 3-D mathematical modeling of PEM fuel cells, part II. Model predictions with liquid water transport, J. Electrochem. Soc. 150 (2003) A1510–A1517.
[17] P. Li, T. Zhang, Q. Wang, L. Schaefer, M. Chyu, The performance of PEM fuel cells fed with oxygen through the free convection mode, J. Power Sources 114 (2003) 63–69.
[18] S. Jemei, D. Hissel, M. Péra, J. Kauffmann, On-board fuel cell power supply modeling on the basis of neural network methodology, J. Power Sources 124 (2003) 479–486.
[19] W. Lee, G. Park, T. Yang, Y. Yoon, C. Kim, Empirical modeling of polymer electrolyte membrane fuel cell performance using artificial neural networks, Int. J. Hydrogen Energy 29 (2004) 961–966.
[20] A. Weber, J. Newman, Transport in polymer electrolyte membranes III. Model validation in a simple fuel cell model, J. Electrochem. Soc. 151 (2004) A326–A339.
[21] S. Um, C. Wang, Three-dimensional analysis of transport and electrochemical reactions in polymer electrolyte fuel cells, J. Power Sources 125 (2004) 40–51.

[22] Y. Ferng, Y. Tzang, B. Pei, C. Sun, A. Su, Analytical and experimental investigations of a proton exchange membrane fuel cell, Int. J. Hydrogen Energy 29 (2004) 381–391.
[23] N. Siegel, M. Ellis, D. Nelson, M. von Spakovsky, A two-dimensional computational model of a PEMFC with liquid water transport, J. Power Sources 128 (2004) 173–184.
[24] H. Meng, C. Wang, Large-scale simulation of polymer electrolyte fuel cells by parallel computing, Chem. Eng. Sci. 59 (2004) 3331–3343.
[25] T. Zhou, H. Liu, A 3D model for PEM fuel cells operated on reformate, J. Power Sources 138 (2004) 101–110.
[26] K. Vafai, C. Tien, Boundary and Inertia Effects on Convective Mass Transfer in Porous Media, Int. J. Heat Mass Transfer 25 (1982) 1183–1190.
[27] K. Vafai, C. Tien, Boundary and inertia effects on flow and heat transfer in porous media, Int. J. Heat Mass Transfer 24 (1981) 195–203.
[28] B. Alazmi, K. Vafai, Analysis of fluid flow and heat transfer interfacial conditions between a porous medium and a fluid layer, Int. J. Heat Mass Transfer 44 (2001) 1735–1749.
[29] C. Lu, A. MacGillivray, S. Hastings, Asymptotic behaviour of solutions of a similarity equation for laminar flows in channels with porous walls, J. Appl. Math. 49 (1992) 139–162.
[30] N. Yang, K. Vafai, Low-density lipoprotein (LDL) transport in an artery- a simplified analytical solution, Int. J. Heat Mass Transfer 51 (2008) 497–505.